CYCLIC BEHAVIOR OF REBAR-PENETRATED CONNECTION BETWEEN GANGUE CONCRETE FILLED STEEL TUBULAR COLUMN AND REINFORCED GANGUE CONCRETE BEAM

Guochang Li[1], Chen Fang[2,*], Xing Zhao[1], Yuwei An[1] and Yu Liu[1]

[1] *School of civil engineering, Shenyang Jianzhu University, Shenyang, 110168, China*
[2] *Department of Civil Engineering, University of Texas at El Paso, El Paso, TX 79968, USA*
**(Corresponding author: E-mail: cfang@miners.utep.edu)*

Received: 31 July 2013; Revised: 22 April 2014; Accepted: 23 October 2014

ABSTRACT: Gangue concrete filled steel tube is a new composite system which has advantages of remarkable earthquake-resistant property and economical efficiency. However, few researches have been done with respect to the behavior of the composite system. Therefore, based on proper material constitutive models and reasonable contact models among different materials, the paper has developed finite element analysis models of rebar-penetrated connection between gangue concrete filled steel tubular column and reinforced gangue concrete beam using software ABAQUS 6.10. Furthermore, finite element analysis results are verified by experiments, demonstrating that the load-displacement curves computed by ABAQUS agree with experimental curves very well and finite element analysis models are reliable to analyze the behavior of the rebar-penetrated connection. Then, these models are used to conduct stress analysis on the composite connection to investigate the failure modes and the force-transferring mechanism. The analysis results show that the rebar-penetrated connection, with full and spindle-shaped load-displacement hysteretic curve, has the reasonable force-transferring route and good energy-dissipation capacity. Finally, the effects of axial load level, stiffness ratio of beam and column, steel ratio and compressive strength of gangue concrete on the behavior of the connection are investigated on the basis of the different models by changing the parameters.

Keywords: Gangue concrete filled steel tubular, Connection, Finite element analysis, Cyclic behavior, Failure mode, Parametric analysis

1. INTRODUCTION

Gangue concrete filled steel tubular (GCFST) column is a new and promising structure in the whole concrete filled steel tubes (CFST) families [1]. The normal concrete is replaced by the gangue concrete to fill in the steel tube. The GCFST column not only keeps advantages of high earthquake-resistant performance of the CFST column, but also possesses prominent merits of less weight and economic efficiency [2]. Owing to less apparent density of the gangue concrete than the normal concrete, the weight of gangue concrete is reduced by as much as 20 percent. More important is that the lateral deformation characteristic of gangue concrete is superior to the normal concrete. It is more helpful to give full play to the confinement effect of the steel tube on the core gangue concrete and improve the bearing capacity of the column [3]. Moreover, the connection between column and beam is the most essential component of the composite column-beam structure. The performance of the connection is key to the accuracy of the force-transferring route and the safety of the whole building [4]. And numerous severe damages of the connections have been occurred around the world, especially in the severe earthquake [5-6]. These damages of the connection resulted in large-loss collapse of the structure. Therefore, it is vital and worthy to investigate the behavior of the connection between GCFST column and reinforced gangue concrete (RGC) beam under the cyclic loading.

In the past years, many designers and scholars proposed different kinds of the connections between CFST column and reinforced concrete (RC) beam and made various researches on these connections. J. Beutel and D. Thambiratnam [7] made an experimental research on the connection

between CFST column and compound beam. Based on the analysis of the failure mode and stress distribution under low cyclic reversed loading, the connection was proved to have high strength and good ductility. Kawaguchi Jun and Morino Shosuke [8] conducted the experiment and finite element analysis on the CFST frame under the vertical reversed loading to analyze the force-transferring mechanism and strength deterioration of the frame. Jian Cai and Chun Yang [9] made an experimental study on the CFST column-beam connection with piercing reinforcing bar to analyze bearing capacity and failure mode. The study showed that the connection has the good and reliable mechanical performance. Guohuang Yao and Yiyan Chen [10-11] proposed a new type of connection between CFST column and RC beam and also made the analysis on the failure process, failure mode and energy dissipation capacity according to experimental research and finite element analysis. However, there is little research on the behavior of the connection between GCFST column and RGC beam. To conduct the study of the connection between GCFST column and RGC beam is an excellent method to fill in the blank of the field.

The paper presents a new type of connection between GCFST column and RGC beam, which can be regarded as a typical rebar-penetrated connection [12]. Based on experimental conditions, the paper creates finite element analysis models of the rebar-penetrated connection between GCFST column and RGC beam. In addition, finite element analysis results are verified by experiments to determine the accuracy of the models. Then, stress analysis on the rebar-penetrated connection is conducted under the low cyclic reversed loading to study the failure modes and force-transferring mechanism. The load-displacement hysteretic curves of the rebar-penetrated connection are calculated and drawn. Finally, the effects of some typical parameters on the behavior of the connection are investigated with different finite element models. The parameters include axial load level, steel ratio, compressive strength of gangue concrete and so forth.

2. FINITE ELEMENT MODEL

2.1 Material Constitutive Model

2.1.1 Gangue concrete

In order to simulate reasonably stiffness deterioration of the concrete, the concrete plastic damage model provided by ABAQUS 6.10 is used to simulate the concrete material [13]. For the compressive zone of the gangue concrete filled in the tube, owing to the constraint effect of tube on the gangue concrete, the gangue concrete is subjected to three-dimensional compressive stress. So the stress-strain relationship curve of the light aggregate concrete filled in steel tube proposed by Bohai Ji [14] is applied to simulation on the property of the gangue concrete filled in tube. For the compressive zone of the unrestrained gangue concrete, the stress-strain relationship curve of light aggregate concrete provided by Southeast University [15] is used, shown in the Figure 1. Because this relationship curve can make the computation easy to converge and also finite element analysis results computed by using the model conform well to the experimental results. The energy fracture criterion [16] can define the softening property of the concrete and enhance the convergence of computation. Hence, the fracture energy (G_f)-crack displacement relation curve is chosen to simulate the property of the gangue concrete in the tensile zone, shown in the Figure 2.

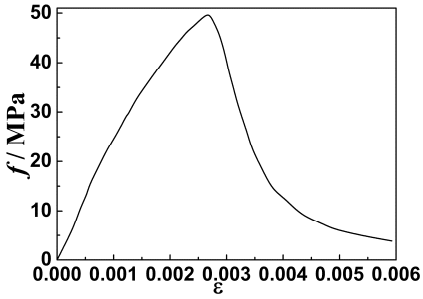

Figure 1. Constitutive Model of Unrestrained concrete

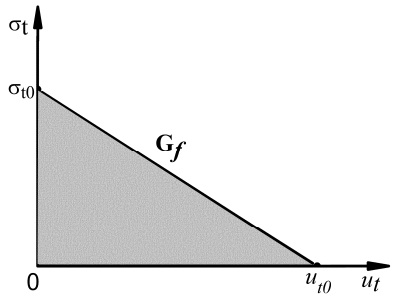

Figure 2. Fracture Energy-crack Displacement Relation Curve

2.1.2 Steel

For the steel of tube and strengthening ring, the stress-strain relationship curve of steel under cyclic loading [17] is applied, shown in the Figure 3. In addition, as Bauschinger effect [18] has an important influence on the bearing capacity of the connection, the Kinematic Hardening model with a von Mises yield surface [19] is applied in the constitutive model of steel. On the basis of many trials and previous researches, the double linear model with bearing capacity deterioration (USTEEL02) in the hysteretic constitutive model collection (PQ-Fiber) proposed by Tsinghua University [20] is used to simulate on the property of the rebar embedded in the gangue concrete beam. The model (USTEEL02) can present the hysteretic behavior of the rebar under cyclic loading and simulate the bond slip between rebar and gangue concrete. In the meanwhile, this model is easy to ensure the convergence of the computation and the accuracy of the finite element analysis results.

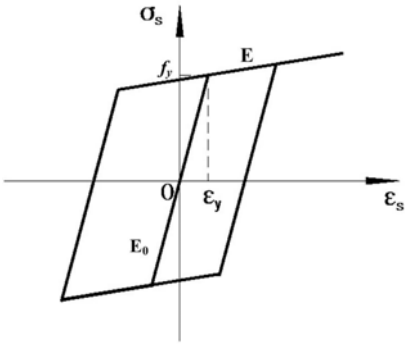

Figure 3. Stress-strain Relation of Steel

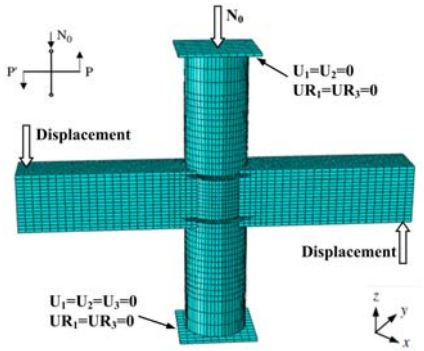

Figure 4. Analysis Model of Rebar-penetrated Connection

2.2 Element and Mesh

The 8-node brick element with reduced integration (C3D8R) is used as the element model to create the gangue concrete. The mapping self-customized meshing is chosen to mesh the gangue concrete. The continuous shell element is used for the steel and the type of element is the four-node conventional shell element with reduced integration (S4R). Truss element is applied to emulation of the rebar embedded in the beam. Figure 4 shows the finite element analysis model of the rebar-penetrated connection. In order to be same as boundary conditions in the experiment, all degrees of freedom except the rotation around y axis in the bottom of the column are constrained. The displacements in x, y direction and the rotations around x, z axes in the top of column are constrained to simulate the pinned connection. During the process of computation, the concentrated force is applied in the top of the column and two displacements with the same magnitude but the opposite direction are applied on both beam ends.

2.3 Contact Model

The contact model between tube and core gangue concrete is composed of the contact in both the normal direction and the tangential direction. Hard contact is adopted to simulate the contact in the normal direction so as to transfer fully the compressive stress between the contact surfaces. Coulomb friction model [21] is applied to simulation of the tangential force. In the model, the penalty friction formula with the elastic slip is used to compute the tangential force. The friction coefficient between the steel and gangue concrete column is taken as 0.6 [22]. As the plate in the top and bottom of the column only transfers the compressive stress in the normal direction, the plate is assumed as elastic plate with large stiffness to simulate the bases. The elastic modulus is defined as 1×10^{12}MPa and Possion's ratio is 0.0001 [23]. The shell-to-solid coupling is used to simulate the contact model between the plate and tube, while the hard contact is applied to contact model between the plate and gangue concrete filled in the tube [24].

3. VERIFICATIONS

3.1 Failure Modes

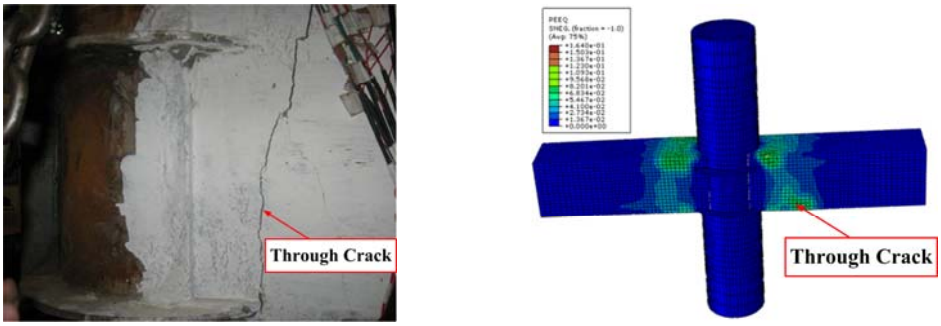

(a) Experiment (b) Finite Element Analysis

Figure 5. Failure Modes of the Rebar-penetrated Connection

Figure 5 shows failure modes of the rebar-penetrated connection in the finite element analysis and the experiment under low cyclic reversed loading. It is clear that, the failure mode received in the finite element analysis achieves a good agreement with those in the experiment. The collapse of the composite structure is due to the shear fracture of the reinforced gangue concrete beam, but the core region of the connection is not out of work and the collapse is not appeared in the GCFST column. This demonstrates that the rebar-penetrated connection between GCFST column and RGC beam has large stiffness and high strength to maintain the safety and stability of the whole building under the severe earthquake. Owing to the plastic hinge in the RC beam, the composite structure is collapsed with the shear fracture. These meet the design ideas of code for seismic design of buildings (GB50011-2010) that "strong column and week beam, strong connection and week members" [25].

3.2 Load-Displacement Hysteretic Curve

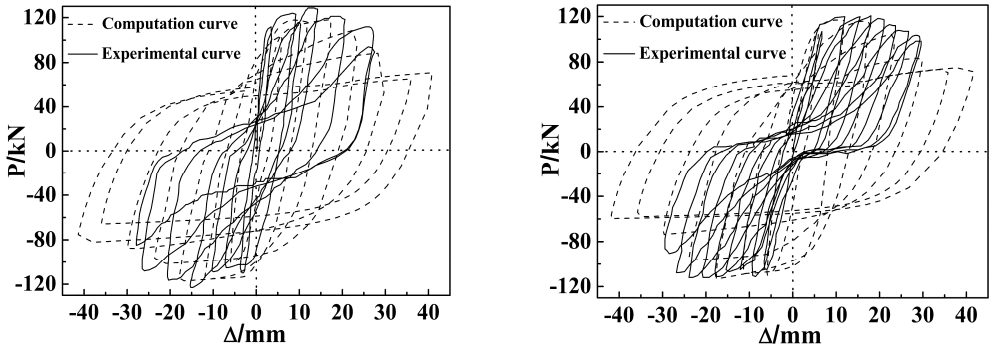

(a)Exterior Connection (b) Interior Connection

Figure 6. Comparison between Experimental Curve and Computation Curve

In order to verify the feasibility of finite element analysis models created using ABAQUS and the accuracy of finite element analysis results, finite element analysis results under low cyclic reversed loading are compared and analyzed with experimental results. Figure 6 shows the comparison of load (P)-displacement (Δ) hysteretic curves of exterior connection with one beam and interior connection with two beams between finite element analysis results and experimental results.

From Figure 6, it is clear that the stiffness and bearing capacity of the connection in the finite element analysis are consistent with the experimental values. However, the experimental curves have the obvious pinch effect phenomenon, while the computation curves are relatively fuller than the experimental curves. So, the shapes of the finite element analysis curves are a little different from experimental curves. But the whole changing trends of finite element analysis curves are accurate and reasonable, which are the same as the experimental curves.

The reasons to result in the difference between finite element analysis curves and experimental curves include: (1) the constitutive model of the gangue concrete used in the paper has some problems in simulating the large bond-slip between rebar and gangue concrete and the crack contact effect of the gangue concrete. At present, few research and analysis are investigated on the constitutive model of gangue concrete. Especially, no studies on the constitutive model of gangue concrete under cyclic loading have been done. However, the crack contact effect of the concrete generated by cyclic load makes a significant influence on the mechanical property of the concrete. Therefore, without the relatively reasonable constitutive model of gangue concrete, it is difficult to make finite element analysis results identical with experimental results. (2) To remedy the defeat of the constitutive model of gangue concrete, the spring model can be used to simulate the bond-slip between rebar and gangue concrete. However, the spring model provided by ABAQUS 6.10 only reflect well the bond-slip under the static loading. Also, the computation convergence is hard to realize with the spring model. As a whole, finite element analysis curves conform well to experimental curves and therefore finite element analysis models are able to complete the research content and purpose.

3.3 Skeleton Curve

Figure 7 shows the comparison of skeleton curves of exterior connection with one beam and interior connection with two beams between finite element analysis results and experimental results.

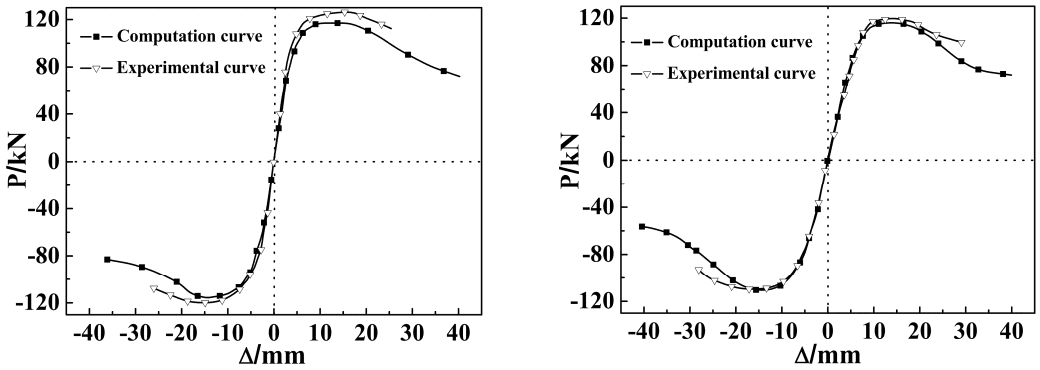

(a)Exterior Connection (b) Interior Connection

Figure 7. Comparison of Skeleton Curves between Experimental Curves and Computation Curves

Figure 7 shows that skeleton curves in finite element analysis are consistent with those in the experiment. The changing trends of finite element analysis curves are the same as experimental curves. Before the peak value of the curve, the curves in finite element analysis are identical with experimental curves. But the values in the finite element analysis are less than experimental values after the ultimate bearing capacity. It is due to the constitutive model of gangue concrete and tie model used to connect the different steel components. Tie model provided by ABAQUS 6.10 has some flaws in simulating the performance of the connection under cyclic loading.

Table 1. Comparison of Characteristic Loads between Experimental Results and Calculation Results

Number		P_0 (kN)	Δ_y (mm)	P_y (kN)	Δ_{max} (mm)	P_{max} (kN)	P_u (mm)
Exterior Connection	Experiment	47.65	5.92	107.4	17.31	122.53	104.5
	Computation	46.58	5.88	103.11	16.88	116.46	98.99
Interior Connection	Experiment	45.2	5.81	108.3	17.27	119.83	99.6
	Computation	44.40	5.85	107.15	17.15	117.53	99.05

NOTE: P_0 represents the cracking load; Δ_y represents the yield displacement; P_y represents the yield load; Δ_{max} represents the maximum displacement; P_{max} represents the maximum load; P_u represents the failure load.

Table 1 shows the comparison of characteristic loads between finite element analysis results and experimental results of the rebar-penetrated connection. The comparative analysis demonstrates that the difference of the bearing capacity between finite element analysis and the experiment is less than 10%. Based on Figure 6 and Figure 7, it is clear that finite element analysis results agree well with experimental results in the elastic stage. After ultimate bearing capacity, finite element analysis results are less than experimental results, but the difference is small. The changing trends of experimental curves and finite element analysis curves are reasonable and accurate. As a result, the models of the rebar-penetrated connection between GCFST column and RGC beam created by ABAQUS 6.10 are accurate and reliable to analyze the cyclic behavior of the rebar-penetrated connection.

4. STRESS DISTRIBUTION

In order to compare stress state of each component in different stages and analyze properly the force-transferring mechanism of the rebar-penetrated connection under cyclic loading, four characteristic points are marked in the hysteretic curve to describe the development of the crack in the gangue concrete [26]. Figure 8 shows the typical P-Δ curve of the connection between CFST column and RC beam. In the curve, A is defined as the point in which has the first crack in the RGC beam. B corresponds to the yield point of the rebar-penetrated connection. C indicates the ultimate bearing capacity (P_{max}) which corresponds to the peak point of the curve. D is the point of failure load (P_u) which is defined as the stage when the load reaches 85% of P_{max}.

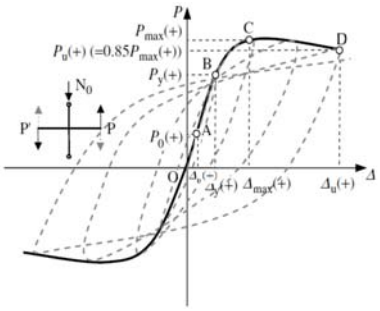

Figure 8. Typical P-Δ Curve

4.1 Gangue Concrete Filled Steel Tubular Column

Figure 9 shows the stress distribution (S33) of the gangue concrete filled in the tube corresponding to characteristic points A, B, C and D. Before the ultimate bearing capacity is reached, with the increase of the cyclic load, the compressive zone of the core gangue concrete filled in the tube develops along the length of the column and the compressive stress increases. In addition, when the constant load is exerted in the top of the column, the lateral deformation of the gangue concrete filled in the tube increases. The increase of lateral deformation results in the increasing confinement effect of the tube on gangue concrete filled in the tube. When the cyclic load arrives at the point C, the maximum compressive stress of the gangue concrete is 44.22MPa which amounts to about 1.86 f_c' and f_c' is the cylinder compressive strength of the gangue concrete. This demonstrates that the tube has an obvious confinement effect on the core gangue concrete and improves the bearing capacity of the gangue concrete to bear the external force. After the ultimate bearing capacity of the connection (point C), the compressive stress of the gangue concrete filled in the tube decreases gradually and then reaches at the failure load (point D).

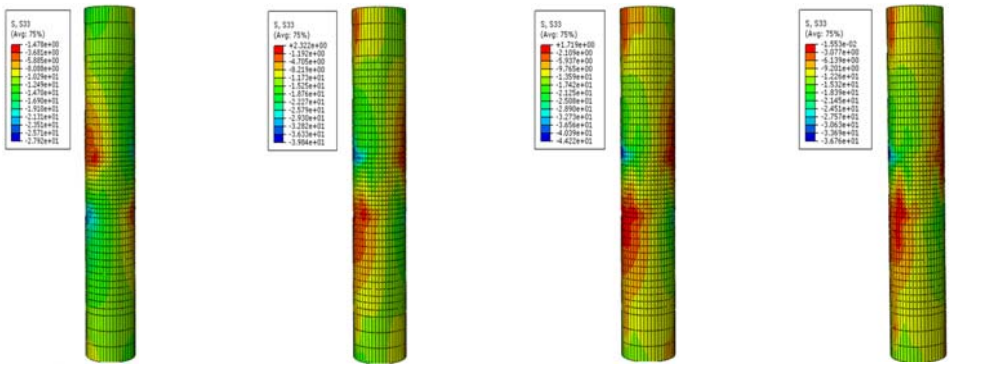

A B C D

Figure 9. Stress Distribution of the Core Gangue Concrete in the Tube (S33)

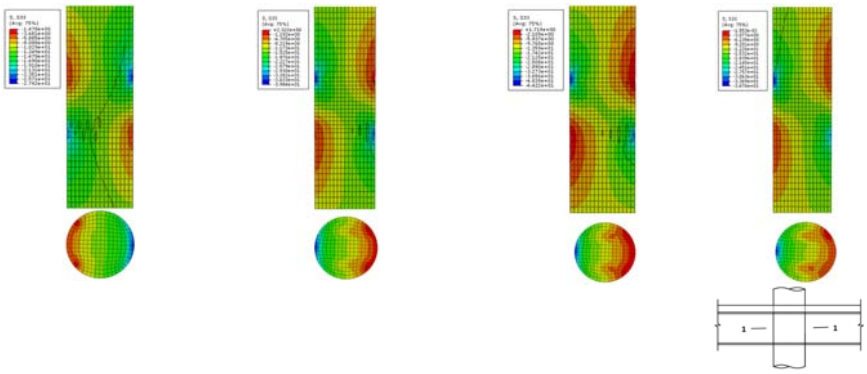

A B C D

Figure 10. Stress Distribution of the Transverse Section of the Core Gangue Concrete (S33)

Figure 10 shows the cut views of the gangue concrete filled in the tube corresponding to each characteristic point. As the cyclic load increases, the neutral axis gradually shifts from the tensile zone to the compressive zone. In the transverse section along the length of the column, the stress distribution with the shape of the diagonal compressive strut is formed obviously in the core area of the rebar-penetrated connection. This demonstrates that the shear stress produced by the cyclic load is undertaken by the core gangue concrete. The compressive strut develops and extends with the increase of the cyclic load before the ultimate bearing capacity, and the average stress of the compressive strut also increases. Owing to the confinement effect of the tube on the gangue concrete, the core gangue concrete is subjected to the tri-axial compressive stress so that the compressive stress of the core concrete reaches the maximum value at the point C. After the point C, the diagonal compressive strut continues developing with the increase of the cyclic load, but the compressive stress of the core concrete decreases due to the damage of the gangue concrete.

Figure 11 shows the vector diagram of the principle stress between column and beam. It is obvious that the diagonal compressive strut with 45 degree is formed to transfer the stress between GCFST column and RGC beam. This demonstrates that the GCFST column undertakes the shear stress produced by the cyclic load and the stress transferring route of the rebar-penetrated connection is clear and reasonable. Figure 12 shows the shear stress distribution (S12) in the core zone of the connection corresponding to each characteristic point. From the Figure 12, the shear stress with the shape of diagonal compressive strut is shown along the diagonal direction in the initial stage of loading. With the increase of the cyclic load, the shear stress gradually increases and the maximum area of the diagonal compressive strut is shown clearly at the point B. After the point B, the shear stress continues increasing and the area of the diagonal compressive strut develops and extends. Finally, a short column with the shape of the diagonal compressive strut is formed in the core zone of the rebar-penetrated connection.

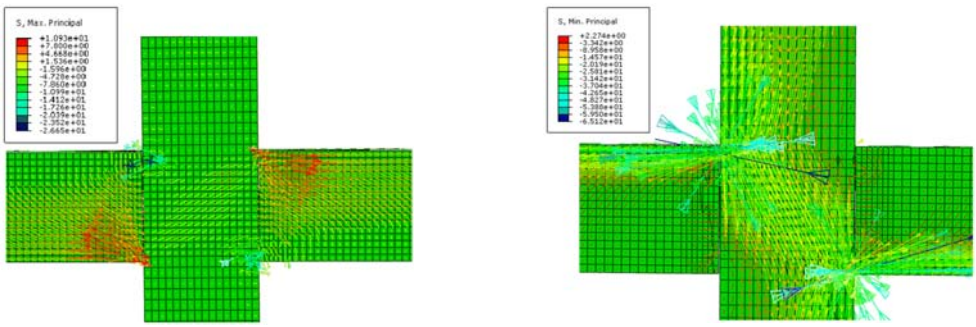

(a) Maximum principal stress (b) Minimum principal stress

Figure 11. Principle Stress of the Rebar-penetrated connection (S. Principle)

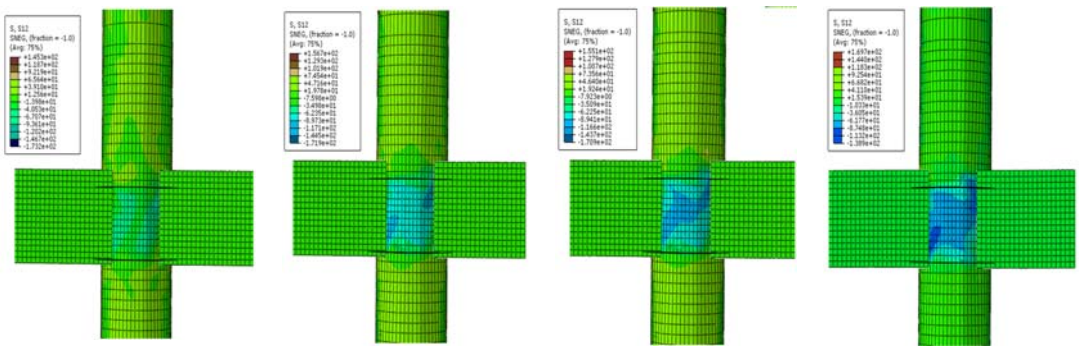

A B C D

Figure 12. Shear Stress Distribution in the Core Zone

Figure 13 shows Mises stress distribution of the steel tube and the strengthening ring. From the Figure 13, in the process of loading, the stress in most parts of the tube is relatively small. It is clear that the stress of the tube is positive. This means the tube has an effective confinement effect on the gangue concrete. The compressive stress and the tensile stress in the tube do not reach the yield strength of the steel. In the process of loading, no obvious buckling is appeared in the tube. The stress of the tube computed in the finite element analysis is consistent with the experimental results.

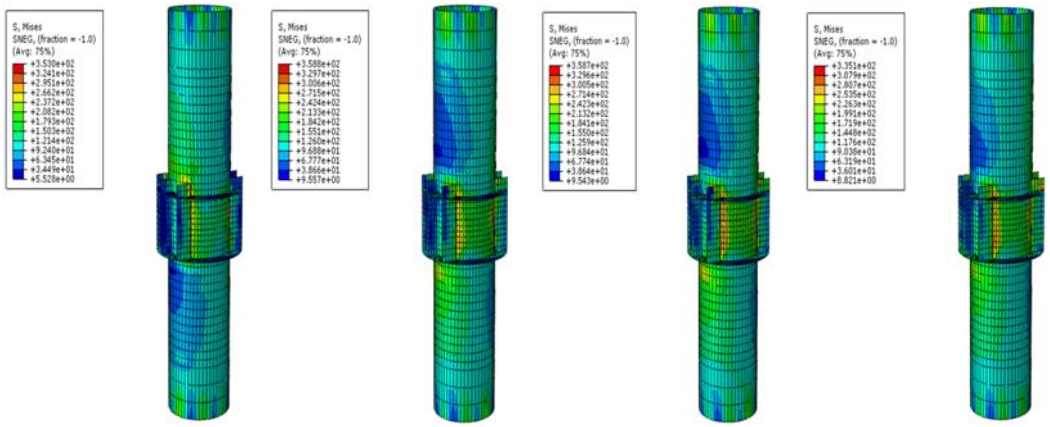

A B C D

Figure 13. Mises Stress Distribution of Tube and Strengthening Ring

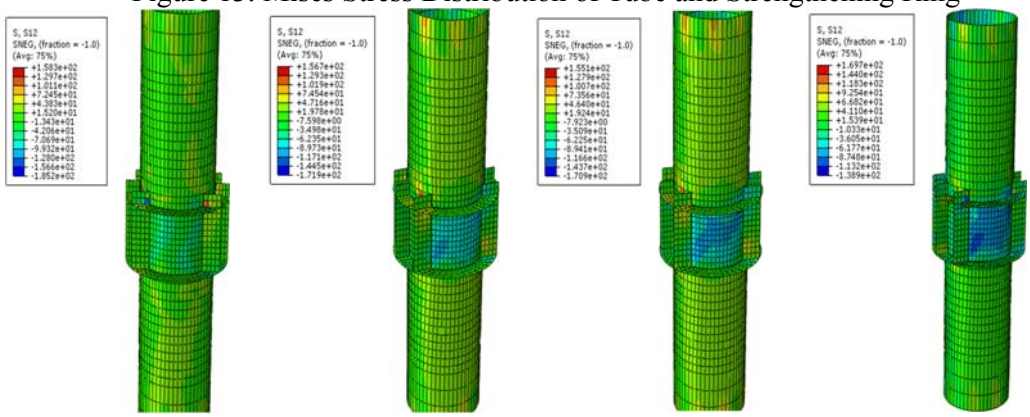

A B C D

Figure 14. Shear Stress Distribution of Tube and Strengthening Ring (S12)

From Figure 13, in the initial stage, the stress in the strengthening ring is small. With the increase of the cyclic load, the stress in the strengthening ring increases gradually and the shear stress in the core zone of the connection also increases. Figure 14 shows the shear stress distribution (S12) of the tube and strengthening ring corresponding to each characteristic point. Based on Figure 12, Figure 13 and Figure 14, when the rebar embedded in the RGC beam is yielded at the point B, the stiffening ring starts to undertake some shear stress under the axial load in the top of column and the bending moment produced by cyclic load. The stress in the strengthening ring is less than the yield strength of the steel and the strengthening ring is working in the elastic stage. It is obvious that the shear stress in the tube is larger than that in the stiffening rib. Therefore, while the stiffening rib is subjected to some bending moments, its primary function is to transfer the bending moment to the GCFST column and the majorities of bending moments produced by cyclic load are undertaken by the GCFST column.

4.2 Reinforced Gangue Concrete Beam

Figure 15 shows the stress distribution (S22) of the GC beam corresponding to each characteristic point. In the initial stage, the tensile zone of the GC beam is very small and the compressive zone develops along the length of the beam with the increase of the cyclic load. In the meantime, the tensile zone develops from the top surface to the middle part in the beam. The maximum stress of the GC beam concentrates on the part in which it is connected to the strengthening ring, and the beam finally collapses in the part. This meets the requirements of the seismic design principle that "strong connection and weak construction members, strong column and weak beam". The development process of the equivalent plastic strain of the GC beam corresponding to each characteristic point is shown in Figure 16. From Figure 15 and Figure 16, it is clear that the initial crack appears in the part of the beam in which it is connected to the strengthening ring. This phenomenon agrees well with the experimental results. With the increase of the cyclic load, the crack is developed along the length of the beam and the width of the crack increases. At the point B, a visible crack is shown in the part of the beam in which it is connected to the strengthening ring. After the point C, owing to the fracture of the gangue concrete, the bearing capacity of the rebar-penetrated connection decreases and the damage is gradually aggravated with the width of the crack increases. At the failure point D, a wide crack, which is penetrated through the depth of the beam, is formed in the same part of the beam. It is clear that the gangue concrete beam collapses, which means the composite structure fails. The development of the crack in the finite element analysis is the same as the experiment phenomenon.

Figure 17 shows stress distribution (S11) of rebar embedded in the GC beam corresponding to each characteristic point. With the increase of the cyclic load, the stress of the longitudinal rebar increases gradually and the shear stress undertaken by stirrup also increases. Under the axial load and the bending moment, the longitudinal rebar is yielded at the point B. This demonstrates that the rebar-penetrated connection is yielded and then enters into the elastic-plastic stage. When point C is reached, the stirrup is yielded under the shear stress and the majority of shear stress is transferred to GCFST column by stiffening ribs. After the point C, the stress of the longitudinal rebar increases, but it does not exceed the ultimate strength of the steel. This illustrates that the bending moment is endured by the longitudinal rebar. Figure 18 shows stress value curve of the longitudinal rebar along the length of beam at point C. It is clear that the maximum stress of the rebar concentrates on the connection part between the beam and the strengthening ring. The maximum value of the stress 415.45 MPa exceeds the yield strength of steel (f_y), but other parts of the rebar still work in the elastic stage. The stress of the longitudinal rebar are identical in the region below the strengthening ring. This demonstrates that the strengthening ring endures some bending moment produced by the cyclic load and therefore the strengthening ring plays an important role in undertaking the bending moment.

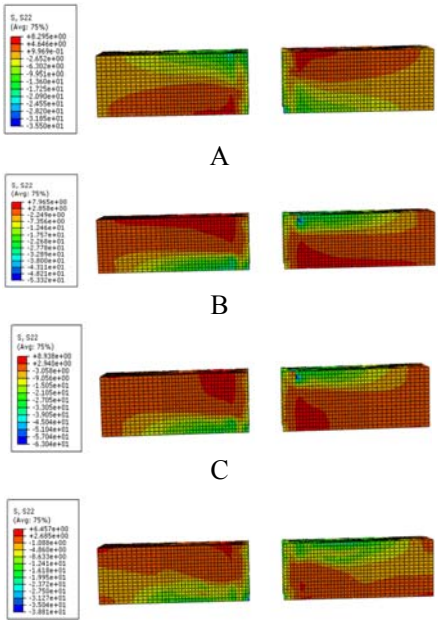

A

B

C

D

Figure 15. Stress Distribution of GC beam

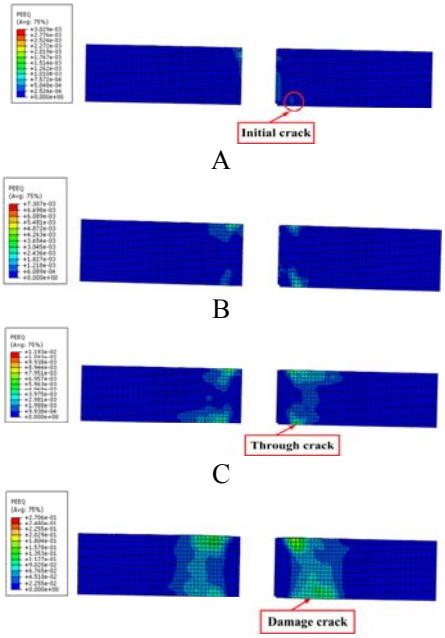

A

B

C

D

Figure 16. Equivalent Plastic Strain of GC beam

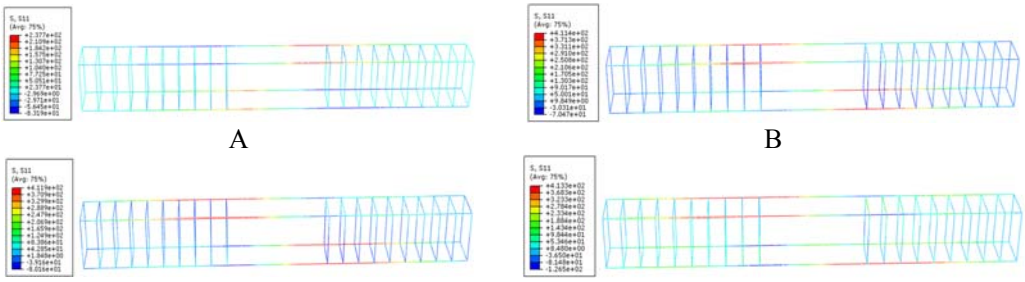

A

B

C

D

Figure 17. Stress Distribution of Rebar (S11)

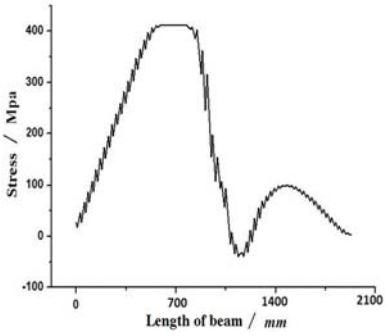

Figure 18. Stress Variation Curve along the Length of Beam

5. PARAMETRIC ANALYSIS

Table 2. Dimensions of the Connection Model

Number	D×t/ mm	*l*/ mm	L/ mm	*d*/ mm	α	*k*	λ	$f_{cu,c}$/ MPa	$f_{cu,b}$ / MPa	N_0/ kN	*n*
J6	325×6	1000	1500	60	0.078	0.853	36	30	30	1800	0.6
J6-*n*-0.2	325×6	1000	1500	60	0.078	0.853	36	30	30	600	0.2
J6-*n*-0.8	325×6	1000	1500	60	0.078	0.853	36	30	30	2250	0.8
J5-α-0.056	325×5	1000	1500	60	0.056	0.853	36	30	30	1800	0.6
J8-α-0.106	325×8	1000	1500	60	0.106	0.853	36	30	30	1800	0.6
J6-*d*-40	325×6	1000	1500	40	0.078	0.853	36	30	30	1800	0.6
J6-*d*-80	325×6	1000	1500	80	0.078	0.853	36	30	30	1800	0.6
J6-$f_{cu,c}$-20	325×6	1000	1500	60	0.078	0.853	36	20	30	1800	0.6
J6-$f_{cu,c}$-40	325×6	1000	1500	60	0.078	0.853	36	40	30	1800	0.6
J6-$f_{cu,b}$-20	325×6	1000	1500	60	0.078	0.853	36	30	20	1800	0.6
J6-$f_{cu,b}$-40	325×6	1000	1500	60	0.078	0.853	36	30	40	1800	0.6
J6-λ-25	325×6	1000	1000	60	0.078	0.853	25	30	30	1800	0.6
J6-λ-49	325×6	1000	2000	60	0.078	0.853	49	30	30	1800	0.6
J6-*k*-1.066	325×6	800	1500	60	0.078	1.066	36	30	30	1800	0.6
J6-*k*-0.711	325×6	1200	1500	60	0.078	0.711	36	30	30	1800	0.6

NOTE: D and t are external diameter and wall thickness of tube; *l* is the length of beam; L is length of column; *d* is the width of strengthening ring; α is steel ratio; k is stiffness of column and beam ratio; $f_{cu,c}$ is cubic compressive strength of gangue concrete in the tube; $f_{cu,b}$ is cubic compressive strength of unrestrained gangue concrete; *n* is axial load level; λ is the slenderness ratio of column.

Based on the stress distribution of the rebar-penetrated connection under low cyclic reversed loading, different finite element analysis models are created by changing the primary parameters to further analyze the behavior of the rebar-penetrated connection and remedy the experimental defects. The primary parameters include the axial load level, compressive strength of gangue concrete, steel ratio, and the width of the strengthening ring. The paper creates 15 finite element analysis models of the rebar-penetrated connection between GCFST column and RGC beam. The material parameters and geometrical parameters are shown in the table 2. Figure 19 shows the bending moment (M)-rotation (θ) hysteretic curves of 15 connections computed by ABAQUS 6.10.

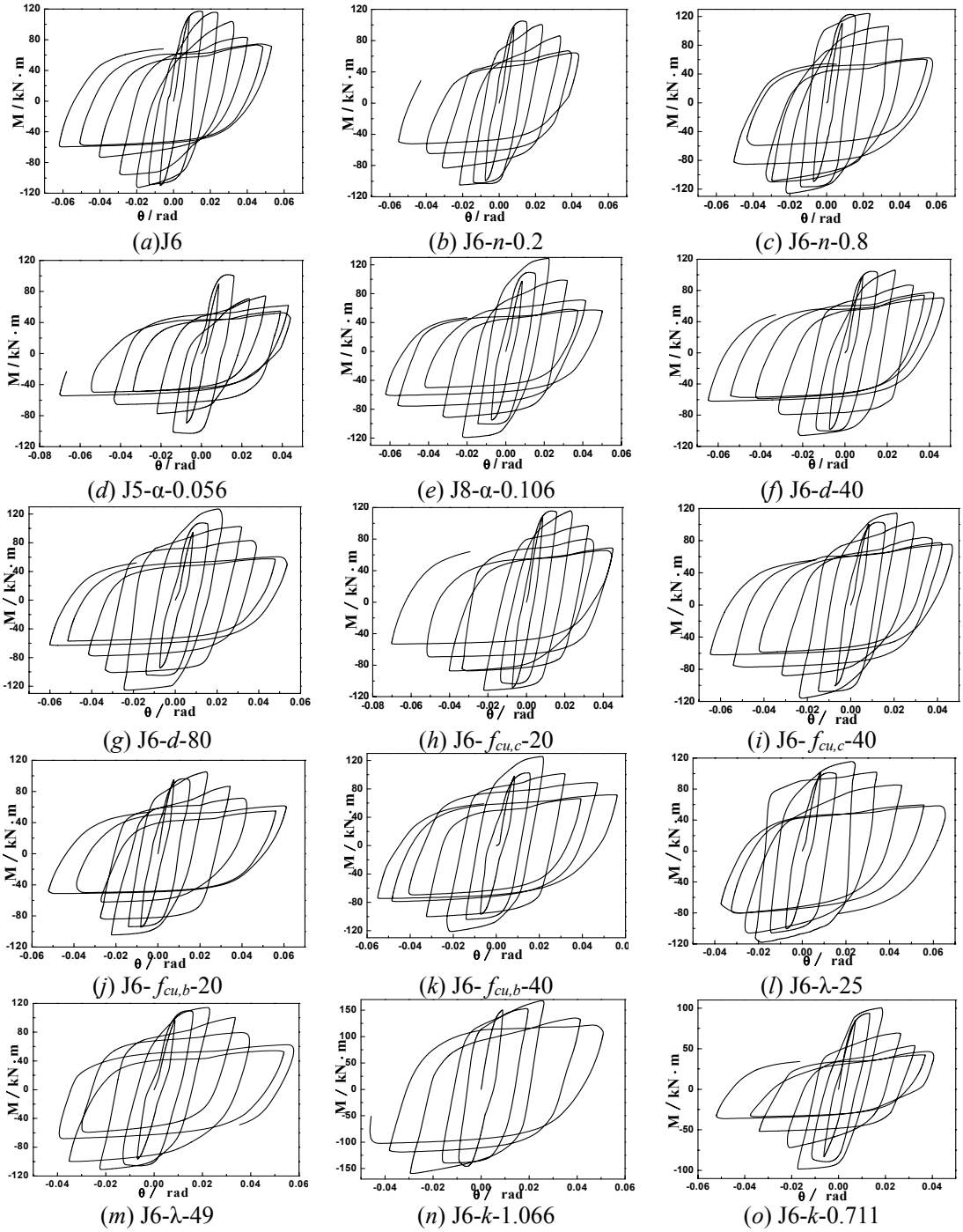

(*a*)J6 (*b*) J6-*n*-0.2 (*c*) J6-*n*-0.8

(*d*) J5-α-0.056 (*e*) J8-α-0.106 (*f*) J6-*d*-40

(*g*) J6-*d*-80 (*h*) J6-$f_{cu,c}$-20 (*i*) J6-$f_{cu,c}$-40

(*j*) J6-$f_{cu,b}$-20 (*k*) J6-$f_{cu,b}$-40 (*l*) J6-λ-25

(*m*) J6-λ-49 (*n*) J6-*k*-1.066 (*o*) J6-*k*-0.711

Figure 19. Bending Moment-rotation Hysteretic Curve of Rebar-penetrated Connection

5.1 Axial Load Level (*n*)

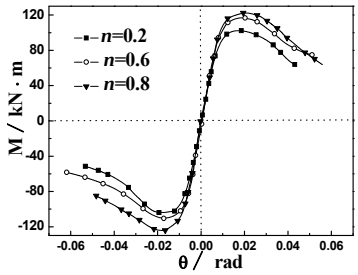

Figure 20. Effect of *n* on *M-θ* Curve

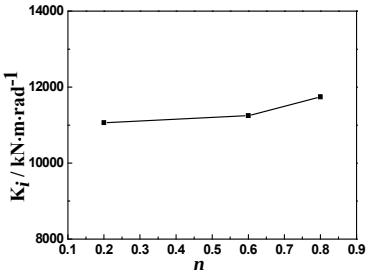

Figure 21. Effect of *n* on Initial Rigidity

Figure 20 shows the effect of the axial load level on skeleton curves of the M-θ curve under the condition to keep other basic parameters unchanged. Figure 21 shows the effect of axial load level on the initial rigidity. Based on Figure 20 and Figure 21, (1) under the cyclic loading, the axial load level has a clear influence on the flexural capacity of the rebar-penetrated connection. As the axial load level increases, the whole curve shifts up and the ultimate flexural bearing capacity increases gradually. (2) In the initial stage, the skeleton curve is almost linear and the length of the elastic stage increases with the increase of the axial load level. The initial rigidity of the connection increases gradually and almost presents the linear increase. (3)With the increase of the axial load level, the rigidity of the connection in the hardening stage increases.

5.2 GCFST Column Steel Ratio (*α*)

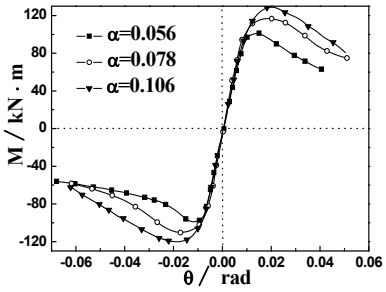

Figure 22. Effect of α on *M-θ* Curve

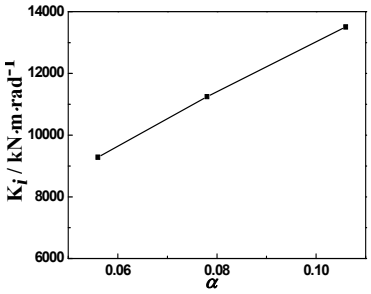

Figure 23. Effect of α on Initial Rigidity

In the paper, the wall thickness of tube is altered to change the steel ratio under the condition to keep other parameters unchanged. Figure 22 shows the effect of different steel ratio on skeleton curve of M-θ curve. Figure 23 shows the effect of steel ratio on initial rigidity. Based on Figure 22 and Figure 23, (1) under the cyclic loading, the connection with larger steel ratio has longer elastic stage and the initial rigidity of the connection with steel ratio of 0.106 is bigger 26% than that of connection with steel ratio of 0.056. Therefore, the steel ratio has a significant influence on the elastic stage of curve. (2)With the increase of the steel ratio, the flexural bearing capacity of the connection increases gradually and the whole curve shifts up without the change of curve shape. As a result, steel ratio has little effect on the shape and variation trend of the curve, but has an obvious influence on the bearing capacity of the rebar-penetrated connection.

5.3 Width of Strengthening Ring (*d*)

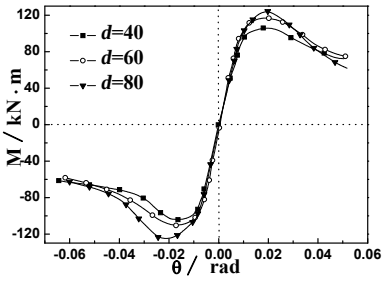

Figure 24. Effect of *d* on *M-θ* Curve

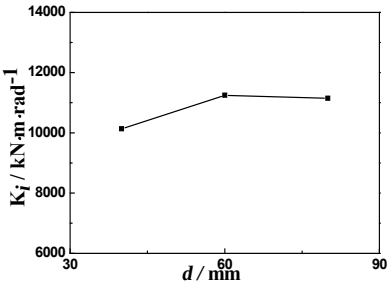

Figure 25. Effect of *d* on Initial Rigidity

Figure 24 shows the effect of the width of the strengthening ring on skeleton curve of the M-θ curve under the condition to keep other basic parameters unchanged. Figure 25 shows the effect of width of the strengthening ring on the initial rigidity. Based on Figure 24 and Figure 25, (1) As the width of strengthening ring increases, the flexural bearing capacity of the rebar-penetrated connection increases, but the shape and variation trend of the curves are barely changed. (2) In the initial stage, the initial rigidity of the connection maintains about 10000kN·m·rad^{-1} and does not change markedly with the increase of the width of strengthening ring. So, the width of strengthening ring has no obvious effect on the elastic stage of the curve. The ultimate flexural bearing capacity increases gradually with the increase of the width of strengthening ring. The ultimate flexural bearing capacity of the connection with the width of strengthening ring of 80 mm increases by 17% more than the connection with the width of strengthening ring of 40 mm, but the initial rigidity of the connection changes barely. As a result, the width of strengthening ring has an obvious effect on the behavior of the rebar-penetrated connection.

5.4 Compressive Strength of Gangue Concrete Filled in the Tube ($f_{cu,c}$)

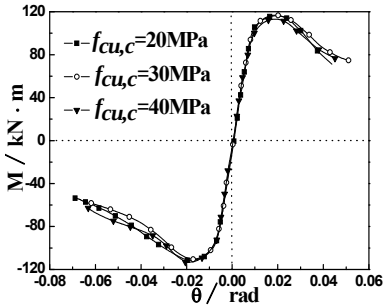

Figure 26. Effect of $f_{cu,c}$ on *M-θ* Curve

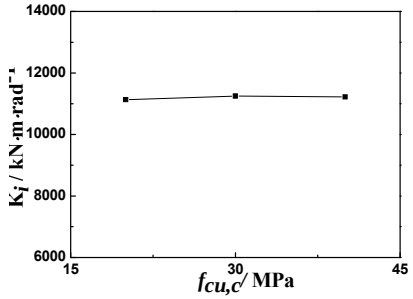

Figure 27. Effect of $f_{cu,c}$ on Initial Rigidity

Figure 26 shows the effect of the compressive strength of the gangue concrete filled in the tube on skeleton curve of the M-θ curve under the condition to keep other basic parameters unchanged. Figure 27 shows the effect of the compressive strength of the gangue concrete filled in the tube on the initial rigidity. Based on Figure 26 and Figure 27, the compressive strength of the gangue concrete filled in the tube has no effect on the mechanical performance of the connection. The shape and changing trend of the curves are not changed with the increase of the compressive strength of the gangue concrete filled in the tube. The initial rigidity of the connection remains unchanged with the change of the compressive strength. The paper focuses on the performance of the connection with the basic design theory "Strong column and weak beam", so the gangue concrete strength has no influence on the bearing capacity of the connection.

5.5 Compressive Strength of Gangue Concrete in the Beam ($f_{cu,b}$)

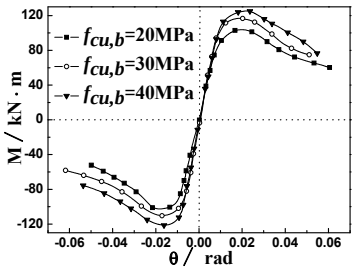

Figure 28. Effect of $f_{cu,b}$ on *M-θ* Curve

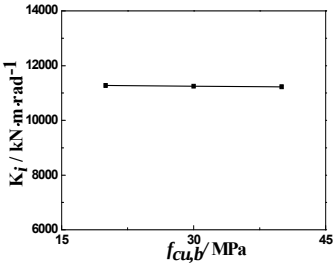

Figure 29. Effect of $f_{cu,b}$ on Initial Rigidity

Figure 28 shows the effect of the compressive strength of gangue concrete in the beam on skeleton curve of the M-θ curve under the condition to keep other basic parameters unchanged. Figure 29 shows the effect of compressive strength of gangue concrete in the beam on the initial rigidity. Based on Figure 28 and Figure 29, (1) As the compressive strength of the gangue concrete increases, the flexural bearing capacity of the rebar-penetrated connection increases, but the shape and changing trend of the curves are barely changed. (2) In the initial stage, the initial rigidity of the connection maintains about 11000kN·m·rad^{-1} and does not change markedly with the increase of the gangue concrete strength in the beam. So, the strength of the gangue concrete in the beam has no obvious effect on the elastic stage of the curve. With the increase of the gangue concrete strength in the beam, the length of the elastic stage increases. The ultimate flexural bearing capacity of the connection increases gradually. Therefore, the compressive strength of gangue concrete has a significant effect on the behavior of the rebar-penetrated connection.

5.6 Slenderness Ratio of GCFST Column (λ)

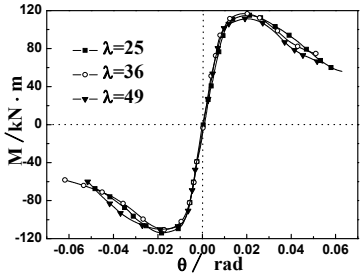

Figure 30. Effect of λ on *M-θ* Curve

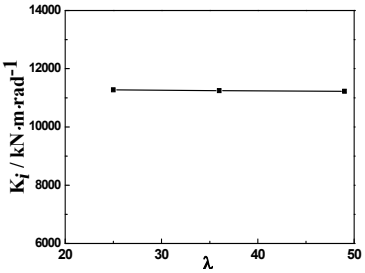

Figure 31. Effect of λ on Initial Rigidity

In the paper, the length of column is altered to change the slenderness ratio of the GCFST column under the condition to keep other basic parameters unchanged. Figure 30 shows the effect of different slenderness ratio on skeleton curve of M-θ curve. Figure 31 shows the effect of slenderness ratio on initial rigidity of the connection. Based on Figure 30 and Figure 31, the slenderness ratio has no effect on the mechanical performance of the rebar-penetrated connection. The shape and changing trend of the curves are not changed with the increase of the slenderness ratio. The initial rigidity of the connection remains identical with the change of the slenderness ratio.

5.7 Stiffness Ratio of Column and Beam (*k*)

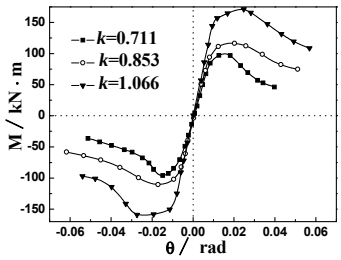

Figure 32. Effect of *k* on *M-θ* Curve

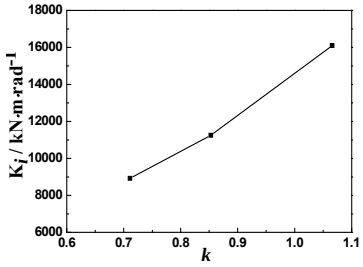

Figure 33. Effect of *k* on Initial Rigidity

In the paper, the length of beam is altered to change the stiffness ratio of column and beam under the condition to keep other basic parameters unchanged. Figure 32 shows the effect of different stiffness ratio on skeleton curve of M-θ curve. Figure 33 shows the effect of stiffness ratio on initial rigidity. Based on Figure 32 and Figure 33, (1) under the cyclic loading, as the stiffness ratio of column and beam increases, the flexural bearing capacity of the rebar-penetrated connection increases and the whole curves shifts up. At the same time, the initial rigidity increases gradually, but the shape and changing trend of the curves are not changed. (2) In the initial stage, the connection works in the elastic stage. With the increase of the stiffness ratio of column and beam, the length of the elastic stage increases and the initial rigidity of the connection increases gradually. The initial rigidity of the rebar-penetrated connection with the stiffness ratio of 1.066 is improved by 70% more than that of the connection with the stiffness ratio of 0.711. (3) As the stiffness ratio of column and beam increases, the ultimate flexural bearing capacity increases and the ultimate flexural bearing capacity of the connection with stiffness ratio of 1.066 is 1.71 times as large as that of the connection with the stiffness ratio of 0.711. As a result, changing the stiffness ratio of column and beam can affect the behavior of the rebar-penetrated connection.

6. CONCLUSIONS

The paper makes finite element analysis on the rebar-penetrated connection between GCFST column and RGC beam to investigate the behavior of the connection under low cyclic reversed loading. The following conclusions are drawn: (1) Based on the comparative analysis on finite element analysis results and experimental results, finite element analysis results are accurate and reasonable so that the finite element analysis models of the rebar-penetrated connection created in the paper can be used to further analyze the behavior of the rebar-penetrated connection. (2) The load-displacement hysteretic curve of the rebar-penetrated connection is full and spindle-shaped. The stiffness degeneration of the rebar-penetrated connection is reasonable. These demonstrate that the rebar-penetrated connection has excellent seismic performance. (3) The strengthening ring is subjected to some bending moments produced by cyclic load and plays an essential function on transferring the bending moment to the GCFST column. The majorities of the bending moment are undertaken by the GCFST column. (4) The maximum stress in the RGC beam concentrates on the part of the beam in which it is connected to the strengthening ring. The beam is collapsed in this part, which fits to the basic seismic design principle “Strong connection and weak members, strong column and weak beam”. (5) In the parametric analysis, axial load level, steel ratio, the compressive strength of the gangue concrete in the beam and the stiffness ratio of column and beam have obvious influences on the bearing capacity of the rebar-penetrated connection, but the shape and changing trend of the curves are not affected. The compressive strength of the gangue concrete filled in the tube and the slenderness ratio of the column has no effects on the behavior of the rebar-penetrated connection.

ACKNOWLEDGEMENT

This project was supported by Liaoning Science Fund (201102177), Technology Program of Ministry of Housing and Urban-Rural Development (2011-k3-23), Liaoning Talents Program (LR2011014).

REFERENCES

[1] Li, G.C. and Zhong, S.T., "Strength and Transverse Deformation Coefficient of Gangue Concrete Filled in the Steel Tube", Journal of Harbin University of Civil Engineering and Architecture, 2002, Vol. 35, No. 3, pp. 20-23.

[2] Li,G.C., Gao, C.F., and Xing, Y.J., "Development on Composite Structure of Steel and Gangue Concrete", Journal of Harbin Institute of Technology, 2003, Vol. 35, pp. 60-62.

[3] Li,G.C., Long, H.B. and Wang, Z.Q., "Inelastic Buckling Load of Gangue Concrete Filled Steel Tubular Middle Long Column under Axial Load", Journal of Shenyang Architectural and Civil Engineering Institute, 2004, Vol. 20, No. 4, pp. 291-293.

[4] Han, L.H., "Concrete Filled Steel Tubular Structure: Theory and Practice", Beijing: Science Press, 2000.

[5] Miller, D.K., "Lessons Learned from the Northridge Earthquake", Engineering Structure, 1998, Vol. 20, No. 4-6, pp. 249-260.

[6] Popov, E.P., Yang, T.S. and Chang, S.P., "Design of Steel MRF Connections before and after 1994 Northridge Earthquake", Engineering Structure, 1988, Vol. 20, No. 12, pp. 1030-1038.

[7] Beutel, A.J., Thambirathnama, D., Pererab, N., "Cyclic Behavior of Concrete Filled Steel Tubular Column to Steel Beam Connections", Engineering Structures, 2002, Vol. 28, No. 24, pp. 29-38.

[8] Kawaguchi, J., Shosuke, M., Hiroshi, A. and Shinya, Y., "Strength Deterioration Behavior of Concrete-filled Steel Tubular Beam-column", Composite Construction in Steel and Concrete II, Proceedings of an Engineering Foundation Conference, 1997, Vol. 1, pp. 825-839.

[9] Cai, J., Yang, C. and Su, H.Q., "Experimental Study of Joints of CFST Column Piercing Reinforcing Bar Hidden Bracket", Industrial Construction, 2003, Vol. 16, No. 3, pp. 61-64.

[10] Yao, G.H., Chen, Y.Y. and Lin, S., "Study on Seismic Performance of a New-type of Concrete-filled Steel Tube Column-RC Beam Joint", Industrial Construction, 2011, Vol. 41, No. 2, pp. 97-102.

[11] Yao, G.H., Chen, Y.Y. and Lin, S., "Finite Element Analysis on a New-type of Concrete-filled Steel Tube Column-RC Beam Joint", Special Structure, 2010, Vol. 27, No. 6, pp. 34-38.

[12] Zhong, S.T., "High-rise Concrete-filled Steel Tubular Construction", Harbin: Heilongjiang Science and Technology Press, 1999.

[13] Yu, T., Teng, J.G., Wong, Y.L. and Dong, S.L., "Finite Element Modeling of Confined Concrete-II: Plastic-damage Model", Engineering Structure, 2010, Vol. 32, No. 3, pp. 680-691.

[14] Ji, B.H. and Yang, M., "Confinement Effect and Strength Criterion of Lightweight Aggregate Concrete Confined by Steel Tube", Bridge Construction, 2006, Vol. 11, No. 4, pp. 11-14.

[15] Zhang, J.W., and Cao, S.Y., "Research on the Stress-strain Curves of Structural Lightweight Aggregate Concrete", Building Science, 2008, Vol. 24, No. 11, pp. 83-85.

[16] 3D Dassault Systems, "ABAQUS Version 6.4: Theory Manual, Users' Manual, Verification Manual and Example Problems Manual", The 3DEXPERIENCE Company, 2003.

[17] Han, L.H., "Concrete Filled Steel Tubular Structures: Theory and Practice (Second Edition)", Beijing: Science Press, 2007.
[18] Li,G.C. and Zhao, B.D., "Analysis of Deflection Process of Gangue Concrete-filled Steel Tubular Member under Bending Moment", Steel Construction, 2003, Vol. 18, No. 1, pp. 19-21.
[19] Boger, R.K., "Non-Monotonic Strain Hardening and its Constitutive Representation", Ph.D. disseration, The Ohio State University, 2006.
[20] Lu, X.Z., Ye, L.P. and Miao, Z.W., "Static-plastic Analysis on Seismic Performance of Construction", Beijing: China Building Industry Press, 2009.
[21] Hu, H.T., Huang, C.S. and Chen, Z.L., "Finite Element Analysis of CFT Columns Subjected to an Axial Compressive Force and Bending Moment in Combination", Journal of Constructional Steel Research, 2005, Vol. 61, No. 12, pp. 1692-1712.
[22] Liu, W., "The Study of Working Mechanism of Concrete Filled Steel Tube under Partial Compression", Journal of Harbin Institute of Technology, 2003, Vol. 35, No. 5, pp. 63-66.
[23] Li, G.C., Fang, C. and Yu, H.P., "Finite Analysis on Performance of Joint between Gangue Concrete Filled Steel Tubular Column with through Rebar and Gangue Concrete Beam under the Monotonic Loading", Applied Mechanics and Materials, 2012, Vol. 204-208, pp. 3724-3730.
[24] Tao, Z., Uy, B., Han, L.H. and Wang, Z.B., "Analysis and Design of Concrete-filled Stiffened Thin-walled Steel Tubular Columns under Axial Compression", Thin-Walled Structures, 2009, Vol. 47, No. 12, pp. 1544-1556.
[25] GB50011-2010, P.R.C. National Standard, "Code for Seismic Design of Buildings", Beijing: China Building Industry Press, 2010.
[26] Qu, H., Tao, Z. and Han, L.H., "Experimental Investigation on Cyclic Performance of CFST Column-RC Beam Joints Enclosed by Rebars", Industrial Construction, 2006, Vol. 36, No. 11, pp. 27-31.